Forecasting a CME by Spectroscopic Precursor?
Solar Physics

D. Baker[1] · **L. van Driel-Gesztelyi**[1,2,3] ·
L.M. Green[1]

Abstract Multi-temperature plasma flows resulting from the interaction be-
tween a mature active region (AR) inside an equatorial coronal hole (CH) are
investigated. Outflow velocities observed by *Hinode* EIS ranged from a few to 13
km s^{-1} for three days at the AR's eastern and western edges. However, on the
fourth day, velocities intensified up to 20 km s^{-1} at the AR's western footpoint
about six hours prior to a CME. 3D MHD numerical simulations of the observed
magnetic configuration of the AR-CH complex showed that the expansion of
the mature AR's loops drives persistent outflows along the neighboring CH
field (Murray *et al.*, 2010, *Solar Phys.*, **261**, 253). Based on these simulations,
intensification of outflows observed pre-eruption on the AR's western side where
same-polarity AR and CH field interface, is interpreted to be the result of the
expansion of a sigmoidal AR, in particular, a flux rope containing a filament
that provides stronger compression of the neighboring CH field on this side of
the AR. Intensification of outflows in the AR is proposed as a new type of CME
precursor.

Keywords: Active Regions, Magnetic Fields, Coronal Mass Ejections

1. Introduction

The Sun is the driver of space weather phenomena such as CMEs. Their impact
on the Earth and the heliosphere in the form of magnetic storms and particle
radiation is considered to be significant especially as eruptive activity in cycle 24
is on the rise. As a result, space weather and its predictability have become key
research areas in solar-terrestrial physics. High-quality observational data from
remote sensing instruments have greatly improved our overall understanding of
the pre-eruptive Sun and our ability to identify CME precursors. What follows

[1] Mullard Space Science Laboratory, University College
London, Holmbury St. Mary, Dorking, Surrey, RH5 6NT, UK
email: db2@mssl.ucl.ac.uk
[2] Observatoire de Paris, LESIA, UMR 8109 (CNRS),
Meudon-Principal Cedex, France
[3] Konkoly Observatory, Budapest, Hungary

is a brief summary, in order of feasibility, of some of the well-documented CME precursors, many of which are strongly related to the magnetic configuration and non-potentiality of the CME source region.

Sigmoids   Sigmoids are forward or reverse S-shaped loop structures observed in EUV and soft X-rays (Rust and Kumar, 1996; Sterling and Hudson, 1997), typically in active regions (ARs) during their decay phase. ARs with a sigmoidal morphology are highly likely to erupt (Hudson *et al.*, 1998; Canfield, Hudson, and McKenzie, 1999; Glover *et al.*, 2000) and when ARs with sigmoids do erupt, at least moderate geomagnetic storms are likely to be produced (Leamon, Canfield, and Pevtsov, 2002). The presence of sigmoids indicates that the magnetic configuration is highly non-potential, sheared, or twisted (*e.g.* Aulanier, Démoulin, and Grappin (2005)). Recent observational studies support the earlier theoretical interpretation that sigmoids are formed by heating along field lines at the periphery of a flux rope embedded in arcade field (Titov and Démoulin, 1999; Green *et al.*, 2007). Observations of sigmoidal loops in an AR prior to its eruption are an indication that a flux rope has formed in the AR prior to CME onset (Green and Kliem, 2009). The strong association of sigmoids with erupting ARs and the ease with which sigmoids are observed especially in X-rays make them a viable CME precursor.

X-ray and EUV Brightenings   Transient brightenings have been long associated with the initiation of CMEs in multi-wavelength observations. Pre-eruption EUV (Dere *et al.*, 1997; Sterling and Moore, 2005) and X-ray brightenings (Harrison *et al.*, 1985; Harrison, 1986; Chifor *et al.*, 2006; Chifor *et al.*, 2007) occur in close proximity to filaments and CME source regions. The timing of the brightenings is of order of minutes to an hour prior to the impulsive phase of flares and the start of the slow-rise phase of a filament/CME eruption (Sterling and Moore, 2005; Chifor *et al.*, 2006; Chifor *et al.*, 2007). Filaments begin to rise in the vicinity of the transient brightenings which occur very close to the polarity inversion line (PIL) at the sites of emerging or cancelling flux. Quadrupolar brightenings observed in TRACE 1600 Å and SOHO CDS O v images are interpreted to be the result of tether weakening in the overlying field, suggestive of the external tether cutting/breakout model (Gary and Moore, 2004; Harra *et al.*, 2005; Williams *et al.*, 2005). Brightenings are created by magnetic reconnection which leads to changes in the magnetic configuration that facilitate subsequent eruptions. Chifor *et al.* (2007) conclude that X-ray precursors are observable signatures in the early stages of eruptions.

Emerging Flux   Systematic studies have shown that emerging flux has a strong correlation with filament eruptions and CMEs (Feynman and Martin, 1995; Green *et al.*, 2003). Feynman and Martin (1995) determined that an important factor in whether a filament erupted was the relative orientation of the new flux with the pre-existing large-scale coronal field. When the flux emergence was oriented favorably for reconnection, the filament erupted, thus, weakening overlying field. Though filament eruptions and CMEs can be linked to flux emergence, it is difficult to connect specific flux emergence events to filament

eruptions since flux emergence occurs everywhere on the Sun (Gopalswamy *et al.*, 2006).

Type-III Bursts and Radio Noise Storms   Type-III radio bursts and noise storms have been identified as possible CME precursors. Type-III bursts are a good indicator of energy deposition along 'open' field lines and storage in the corona prior to a major eruption (Jackson *et al.*, 1978) and they are indicative of pre-eruption instabilities in the large-scale structure that eventually erupts (Gopalswamy *et al.* (2006), Pick *et al.* (2006), and references therein). Radio noise storms originating from persistently non-thermal accelerated particle populations in the coronal fields of ARs have been found to precede CMEs (Gopalswamy *et al.* (2006), Chen, Innes, and Solanki (2008), and references therein).

Prominence Oscillations   Prominence oscillations were first observed in Hα (Ramsey and Smith, 1966). Such oscillations can be caused by any number of triggers including eruptive MHD instabilities, fast-mode blast waves, photospheric convection, and photospheric/chromospheric oscillations (Vršnak, 1993). Chen, Innes, and Solanki (2008) and Foullon, Verwichte, and Nakariakov (2009) observed continuous oscillations for hours preceding the eruption of a prominence as a CME. Chen, Innes, and Solanki (2008) argue that 90% of CMEs are associated with prominences therefore prominence oscillations are a viable CME precursor.

One of the major discoveries made by EIS was the presence of persistent blue-shifted emission in coronal lines observed at the periphery of ARs. The AR outflows exhibit a common set of characteristics including line-of-sight (LOS) velocities from a few to 50 km s^{-1} (Harra *et al.*, 2008; Del Zanna, 2008; Doschek *et al.*, 2008), and locations in regions of low electron density and low radiance (Del Zanna, 2008) at the edges of the AR over monopolar magnetic field concentrations (Sakao *et al.*, 2007; Doschek *et al.*, 2008; Baker *et al.*, 2009a). Recent work by Bryans, Young, and Doschek (2010), Peter (2010), and Brooks and Warren (2011) suggests that portions of AR outflows may be comprised of multiple component outflows with velocities as high as 200 km s^{-1} in Fe XII, Fe XIII, and Fe XV emission lines. The blue-shifted plasma flows are believed to be a possible source of the slow solar wind (Sakao *et al.*, 2007; Harra *et al.*, 2008).

Here a novel type of CME precursor based on changes in AR outflows is reported. Approximately six hours prior to a CME eruption, intensification of plasma outflows from the periphery of a sigmoidal AR embedded in an equatorial coronal hole (CH) was observed by EIS. In Section 2, we detail the imaging and spectroscopic data used in this investigation. We recount the multi-instrument coronal observations of the AR-CH complex and magnetic field evolution leading to a CME in Sections 3 and 4, respectively. Multi-temperature AR outflows and the striking intensification of these outflows from the western side of the AR are described in Section 5. Section 6 contains a summary of all observations. In Section 7, the key results from 3D MHD simulations of the AR-CH complex
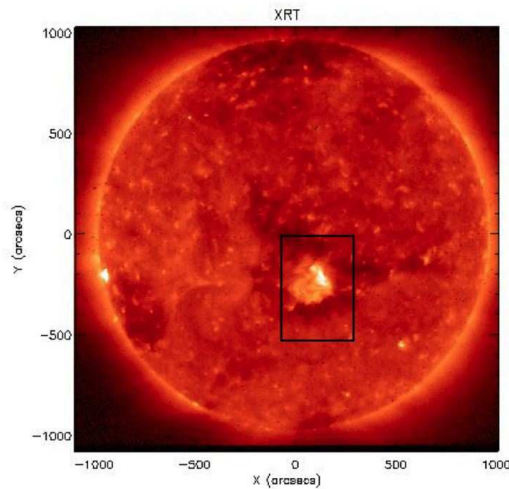
Figure 1. *Hinode* XRT thin Al mesh full disk image overlaid with the EIS FOV showing the AR-CH complex at the solar central meridian on 17 October 2007 at 17:48 UT.

are detailed and, in Section 8, we discuss whether the compression of plasma along neighboring CH field resulting from AR expansion explains the observed intensification of AR outflows prior to a CME.

2. Data Analysis

The focus of this study is to analyze multi-temperature plasma outflows of an AR embedded in a surrounding CH to determine why outflow velocities nearly doubled after three days of remaining unchanged. EIS (Culhane *et al.*, 2007) provided the means to methodically examine these plasma flows. Other instruments are used to provide context information, magnetic field evolution, AR loop structure and evolution, and coverage of a CME attributable to the AR. The AR was not given a NOAA number (no spots observed), but it was visible on the solar disc from 11 to 23 October 2007.

EIS has high spectral resolution that allows for accurate measurements of Doppler shifts in a wide range of lines formed at temperatures characteristic of the transition region (TR) and the corona. The observations consist of rasters using both the $1''$ and $2''$ slits stepped from solar west to east. Rasters contain from 15 to 24 spectral lines, depending on the study. Table 1 summarizes the EIS raster details including the field-of-view (FOV), exposure times, and total raster time for each study. The quality of the velocity data varies with exposure time and slit size. Unfortunately, none of the EIS studies were designed for simultaneous observation of a high-radiance AR and a low-radiance CH which is

Table 1. Details of EIS observations.

Date (2007)	Time (UT)	Study (No.)	Slit	Exp. time (s)	FOV	Raster time (h)	Ref. wvl method[1]
15 Oct	20:39	46	$1''$	15	$256'' \times 256''$	1.1	Ave
16 Oct	02:17	46	$1''$	15	$256'' \times 256''$	1.1	Ave
16 Oct	03:28	46	$1''$	15	$256'' \times 256''$	1.1	Ave
16 Oct	04:39	46	$1''$	15	$256'' \times 256''$	1.1	Ave
16 Oct	21:11	205	$1''$	45	$360'' \times 512''$	2.3	QS
17 Oct	00:26	205	$2''$	45	$360'' \times 512''$	2.3	QS
17 Oct	02:47	205	$2''$	45	$360'' \times 512''$	2.3	QS
18 Oct	00:18	198	$1''$	45	$460'' \times 384''$	5.1	QS

[1]Ref. wvl method refers to how the reference wavelength was determined. Ave is the average wavelength of the data cube and QS is the average wavelength for a region of quiet Sun.

a challenging task. Most of the Doppler shift results are obtained from EIS's Fe XII 195 Å core line. Fe XII 195 Å is most suitable for line profile measurements because good count rates are available for bright AR features and the low intensity CH. However, count rates for hotter lines such as Fe XV 284 Å in the CH were not sufficient for short exposure, $1''$ slit rasters.

Raw spectral data were corrected for dark current, hot pixels, warm pixels, and cosmic rays using standard procedures in SolarSoft (*e.g.* eis_prep and eis_auto_fit). Calibrated spectra were fitted with double Gaussians to the Fe XII emission line profiles. In the outflow regions, less than 0.16% of the pixels were well represented by a double gaussian fit. See Bryans, Young, and Doschek (2010) for the method used here. Instrumental effects such as orbital variation, slit tilt, and CCD detector offset were corrected and the reference wavelengths were taken either from the average value obtained in a relatively quiescent Sun region of the rasters or the average of the data cube, depending on the raster (see column 8 of Table 1).

STEREO 195 Å, TRACE 171 Å, SOHO MDI, and *Hinode* XRT (Wuelser *et al.*, 2004; Handy *et al.*, 1999; Scherrer *et al.*, 1995) data were prepared and calibrated using standard instrumental procedures in SolarSoft. In addition, MDI magnetograms were corrected for the difference between LOS and assumed radial field using the `zradialize` routine.

3. Coronal Observations

The evolution of the AR within an equatorial CH was tracked using multi-wavelength observations over a four day period spanning 15 to 18 October 2007. To give context of the size and location of the AR-CH complex, Figure 1 shows a full disk X-ray image on 17 October at 17:48 UT from *Hinode* XRT (Golub *et al.*, 2007). The AR was associated with a slow coronal mass ejection (CME) of 371 km s^{-1} as viewed in the plane of the sky by the Large Angle and Spectroscopic

Coronagraphs (LASCO) (Brueckner *et al.*, 1995) on board SOHO. The CME was located in the southwestern quadrant of the LASCO C2 difference image timed at 09:06 UT on 18 October 2007 (http://cdaw.gsfc.nasa.gov/CME_list/). There were no significant GOES X-ray flares detected with the CME.

The CME onset can be determined from STEREO EUVI 195 Å images. At approximately 07:05 UT, the AR's loops start to brighten towards the west as viewed in Figure 2, top panel. By 08:10 UT, the expanded AR loop structure is rotating in a counter-clockwise direction along the southwestern perimeter coincident with the formation of a small dimming region (red arrow) at the AR's center in the bottom panel of Figure 2. The loop structure continues to expand and rotate as the AR erupts until approximately 09:00 UT when the bright arcade of loops spanning the PIL where the eruption occurred begins to form (yellow arrows in the bottom panel of Figure 2). See the supplement to the electronic version of the article for a STEREO EUVI 195 Å movie.

The presence of a filament is evident in TRACE 171 Å data on 17 and 18 October. Figure 3, left panel, shows the smoothly curved reverse S-shaped filament located in the northeastern quadrant of the AR along the main PIL, indicated with yellow arrows. Prior to the CME, from 04:47 to 05:01 UT on the 18th, plasma is flowing along the filament (though there are gaps on either side of this period in the TRACE data). During the onset of the CME eruption, the filament developed a kink as indicated in the right panel of Figure 3.

On 18 October, prior to the CME, a clear reverse-S sigmoid-shaped loop structure is evident in X-rays as viewed in Figure 4. The presence of the reverse-S sigmoid indicates that a flux rope with left-handed chirality is present in the AR (Pevtsov, Canfield, and McClymont, 1997). The counter-clockwise rotation of the AR loop structure observed in STEREO EUVI 195 Å images is consistent with the reverse-S sigmoid, therefore, left-handed flux rope (Green *et al.* (2007) and references therein). In fact, the rotation is observed at multiple coronal temperatures ranging from EUV to soft X-rays.

4. Magnetic Field Evolution

The small AR was measured to have magnetic flux of approximately 3×10^{21} Mx as it crossed the solar central meridian. On 14 October, the following AR polarity (positive) has started to break up and disperse while the leading polarity (negative) remained essentially concentrated. By early on the 15th, the negative field has fragmented as well. It is clear that the AR is in the decay phase of its evolution. Figure 5 displays a series of MDI magnetograms on 17 and 18 October leading up to/during/after the CME eruption.

The filament identified in TRACE 171 Å images lies along the PIL in the northwestern quadrant of the AR. Opposite polarity flux converges at two different locations along the PIL from early on the 17th as indicated by the arrows in Figure 5. These two locations lie along a supergranular cell boundary where both polarities are found. Frequency of flux convergence and subsequent cancellation events increase leading up to the CME eruption on the 18th when opposite polarity flux converges beneath the filament preceding the eruption.
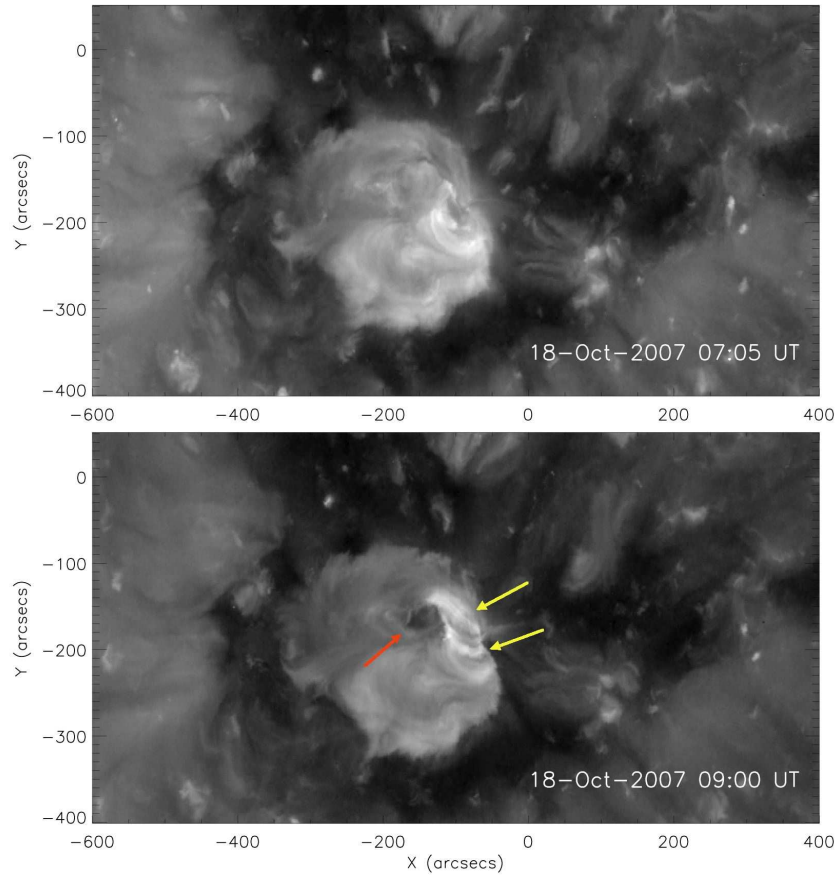
Figure 2. STEREO A 195 Å images of the AR in a low-latitude CH about 30 mins before and 1.5 h after the onset of the CME eruption. The red arrow indicates a dimming region and the yellow arrows identify the post-eruption loop arcade, both of which are classic post-CME signatures.

Flux cancellation also occurs at the boundary of the included positive polarity (red line) but the strongest cancellation is along the PIL (yellow arrow) where flux density is highest. The brightening of the X-ray sigmoidal loop structure occurs above the site of the strongest cancellation just prior to the eruption.

The location of the AR in a CH provided a unique opportunity to measure flux cancellation with a high degree of confidence. Typically, flux changes are difficult to measure in an AR located in the quiet Sun or nested amongst other ARs due to the mixing of magnetic fragments. In the AR-CH complex, the positive polarity of the AR is easy to identify in the negative polarity CH so that the change in flux over time can be determined by simply setting a contour around the positive polarity fragments and measuring the positive flux contained within the contour. Figure 6 shows the evolution of AR flux determined from
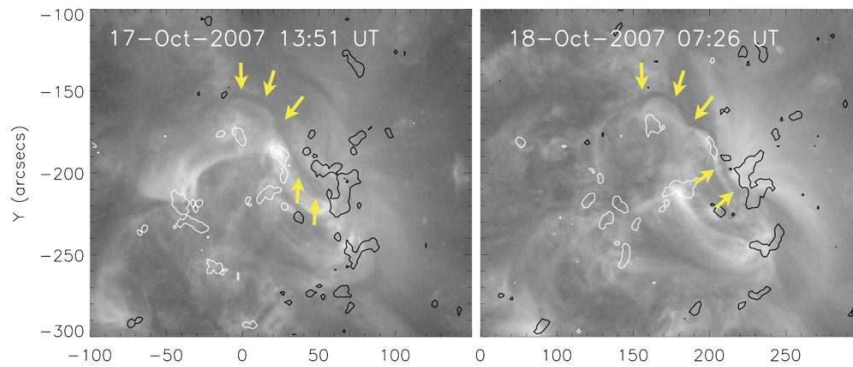
Figure 3. TRACE 171 Å images of the AR in a CH 19 hours (left panel) and minutes (right panel) before the CME, respectively. The filament, indicated by yellow arrows, develops a kink minutes before the eruption. MDI magnetic field contours white/black $\pm$ 100 G (gauss) are overlaid on both images.

SOHO MDI magnetograms from 14 to 19 October. On average 9.7% of the flux per day is removed from the AR in the four days leading up to the CME eruption.

5. Active Region Outflows

In the next section, multi-temperature plasma flows at 02:47 on 17 October are investigated. This is followed by an analysis of AR outflows in Fe XII emission for four days from 15 to 18 October.

5.1. Multi-temperature EIS Intensity and Velocity Maps - 17 October 2007 at 02:47 UT

Figures 7 and 8 show a range of emission line intensity (left) and velocity (right) maps of this unique set of AR-CH observations for 17 October at 02:47 UT. The coolest line is He II 256.32 Å with a temperature of $10^{4.7}$ K (Young *et al.*, 2007). This line is one of the strong EIS lines, however, it is a complex blend of much higher temperature Si X, Fe XII, and Fe XIII emission lines ($T = 10^{6.1}$ K, $10^{6.2}$ K, and $10^{6.1}$ K, respectively; Young *et al.*, 2007). It is likely that the bright loops are of the higher temperature blends as the same feature is visible in hotter Fe ions intensity maps. The He II velocity map is dominated by red-shifted downflows in the AR. The surrounding CH is a mix of downflows and blue-shifted outflows though blue-shifts are more characteristic of this region. Mg VII 278.39 Å and Si VII 275.35 Å lines have similar formation temperatures ($10^{5.8}$ K; Young *et al.*, 2007) and, as expected, common features are found in their intensity and velocity maps. Red-shifted, low lying compact loops are located in the core of the AR. A comparison of Si VII and Mg VII (blended with Si VII) velocity maps confirms that the lines have similar strength signals (or counts) in EIS AR spectrum as the red-shifted loops appear roughly the same, however, the Si VII has a stronger signal in the EIS quiet Sun spectrum so the CH portion of velocity map is more
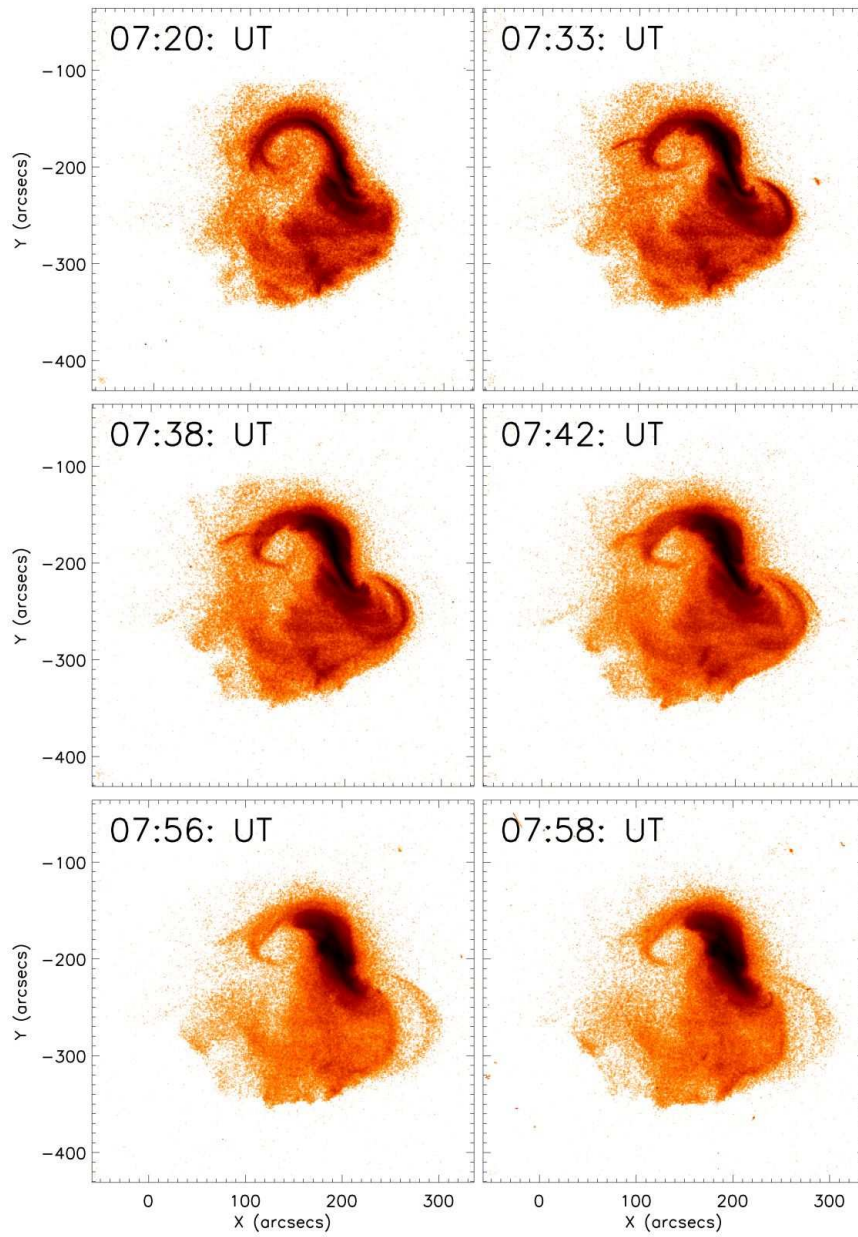
Figure 4. *Hinode* XRT thin Be filter images of the AR's sigmoidal structure on 18 October at the time of the CME eruption. The expansion of the flux rope and rotation of the structure during the eruption are evident from 7:33 UT. The bright sigmoid is located over the region of most intense magnetic flux cancellation (*cf.* yellow arrows in Figure 5).
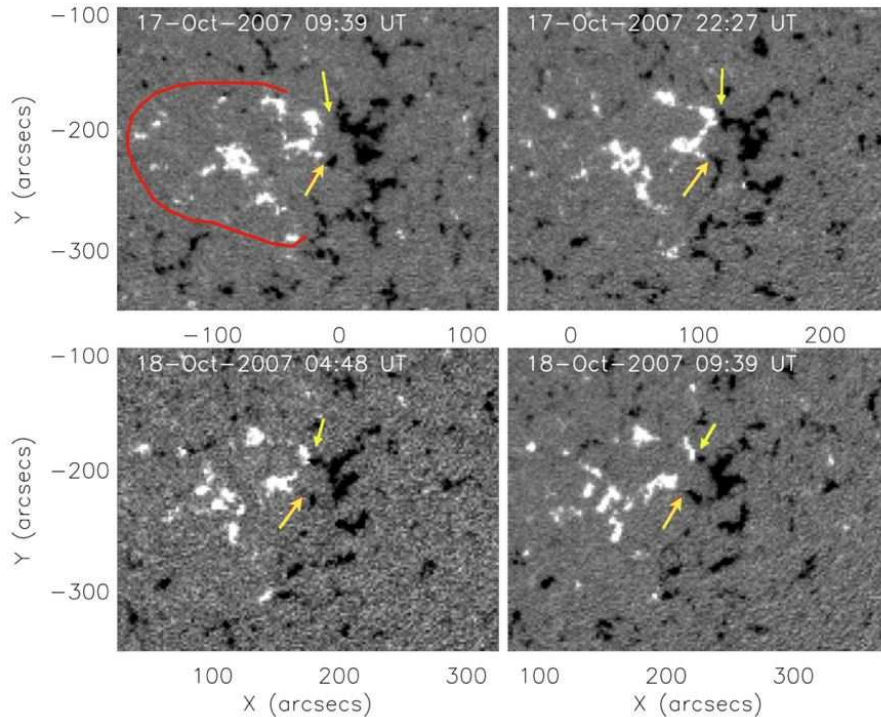
Figure 5. SOHO MDI magnetograms of magnetic field evolution indicating the region of principal flux cancellation along the main PIL of the AR (yellow arrows). Note that a lower level of flux is cancelling along the boundary of the included positive polarity (approximately indicated by the red line in the upper left panel).

distinct. Whereas the cooler chromospheric and TR lines are dominated by red-shifted downflows, hotter coronal lines have definite blue-shifted outflows at the periphery of the AR. The blue-shifted outflow regions appear to expand with temperature as is evident when comparing velocity maps of Fe x 184.54 Å, Fe xii 195.12 Å, and Fe xiii 202.04 Å ($T = 10^6$ K, $T = 10^{6.1}$ K, and $T = 10^{6.2}$ K, respectively; Young *et al.*, 2007) in Figure 8. The outflow regions fan out and velocities increase with temperature (Del Zanna, 2008). In this data set the hotter Fe ions also have very bright extended loop structures in common. Fe x and Fe xiii are unblended lines, however, Fe xii is self-blended at 195.18 Å (Young *et al.*, 2009) and is at the peak of the EIS sensitivity curve so is the strongest emission line observed by EIS (Young *et al.*, 2007).

5.2. Fe xii EIS Observations - 15 to 18 October 2007

In the previous section, multi-temperature intensity and velocity maps of a single EIS observation were described. Here, only the strong EIS Fe xii 195 Å emission line plasma flows are compared over four days. In the velocity maps,
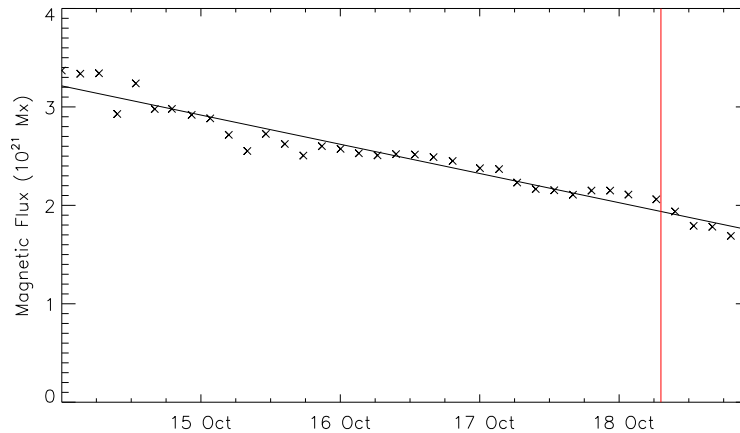
Figure 6. AR positive flux from 00:03 UT on 14 October to 00:03 UT on 19 October. On average 9.7% of the total flux per day is removed from the AR over the four day period leading up to the eruption at approximately 07:30 UT on 18 October. The CME onset is indicated by the vertical red line.

there is a series of loop structures connecting positive to negative magnetic field concentrations at the AR's footpoints. The loops are red-shifted, indicating downflows within the loop structures. Downflows are persistent in the AR's loops throughout the observation period. LOS downflow velocities range from a few km s^{-1} up to a maximum of 35 km s^{-1}. EIS He II, Si VII, and Mg VII velocity maps in Figure 7 are typical of the rasters. See the supplement to the electronic version of the article for EIS intensity and velocity maps for all rasters. Velocity maps are overlaid with SOHO MDI magnetic field contours of $\pm$ 100 G (gauss) (white/black contours).

Blue-shifted outflow regions are observed at the periphery of the AR located over the magnetic field concentrations of the AR's footpoints. Outflows are clearly visible on both sides of the AR. The western outflow region has formed a rosette-like shape with outflows tracing the dense footpoint structure. On the eastern side, the AR looks similar to a sea anemone. The anemone structure is characterized by loops that connect the AR's positive polarity and the opposite polarity of the surrounding monopolar CH (Shibata *et al.*, 1994; Asai *et al.*, 2008; Asai *et al.*, 2009; Baker *et al.*, 2009b). The eastern outflows originate from a region in the middle of the anemone structure.

5.3. Intensification of AR Outflows on 18 October 2007

Blue-shifted velocities in the core eastern and western outflow regions remained stable from approximately a few to 13 km s^{-1} from the 15 to 17 October. Though the AR evolved during this period, overall, the location of the eastern and western outflows continued to originate from the periphery of the AR, over
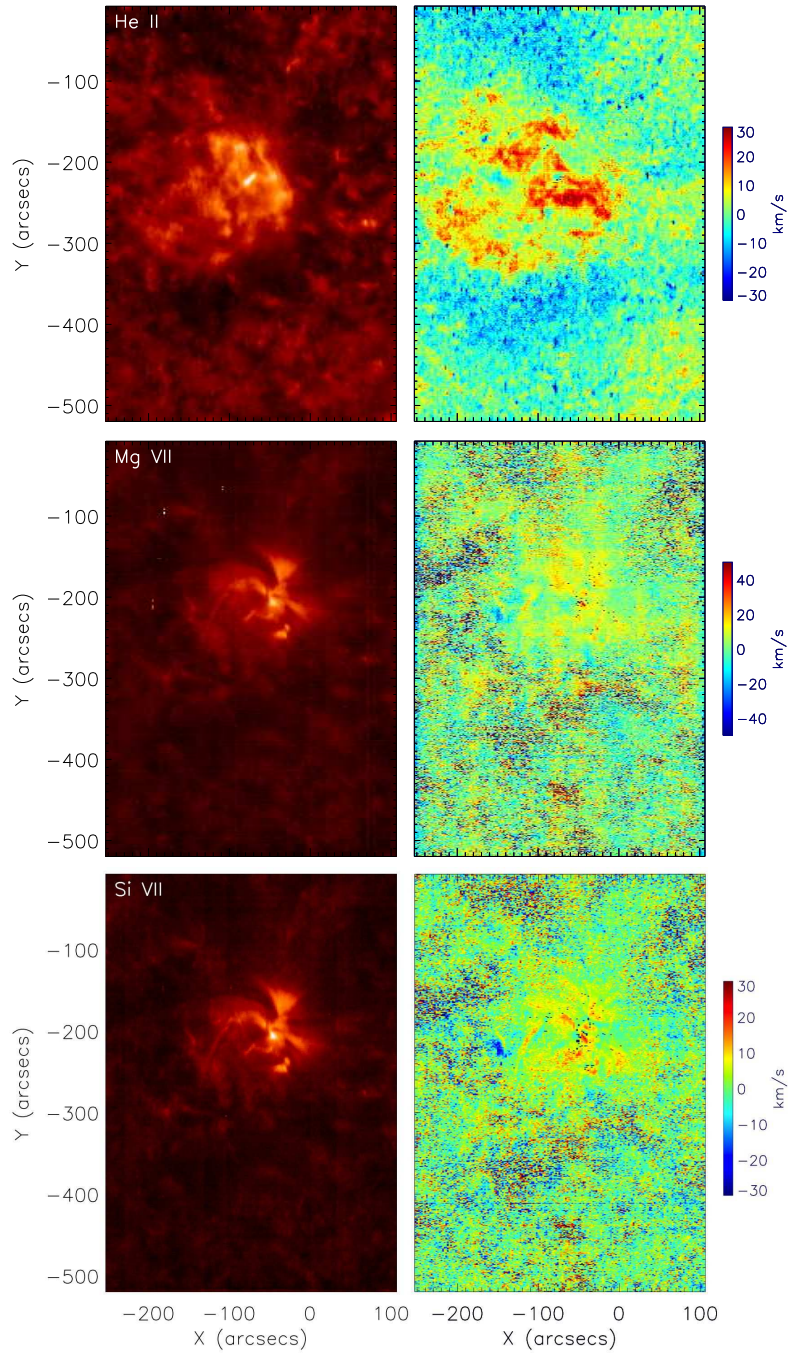
Figure 7. He II, Mg VII, and Si VII intensity (left) and velocity (right) maps on 17 October 2007 02:47 UT. AR outflows are not evident at lower formation temperatures. Velocity maps are characterized by red-shifted, low compact loops.
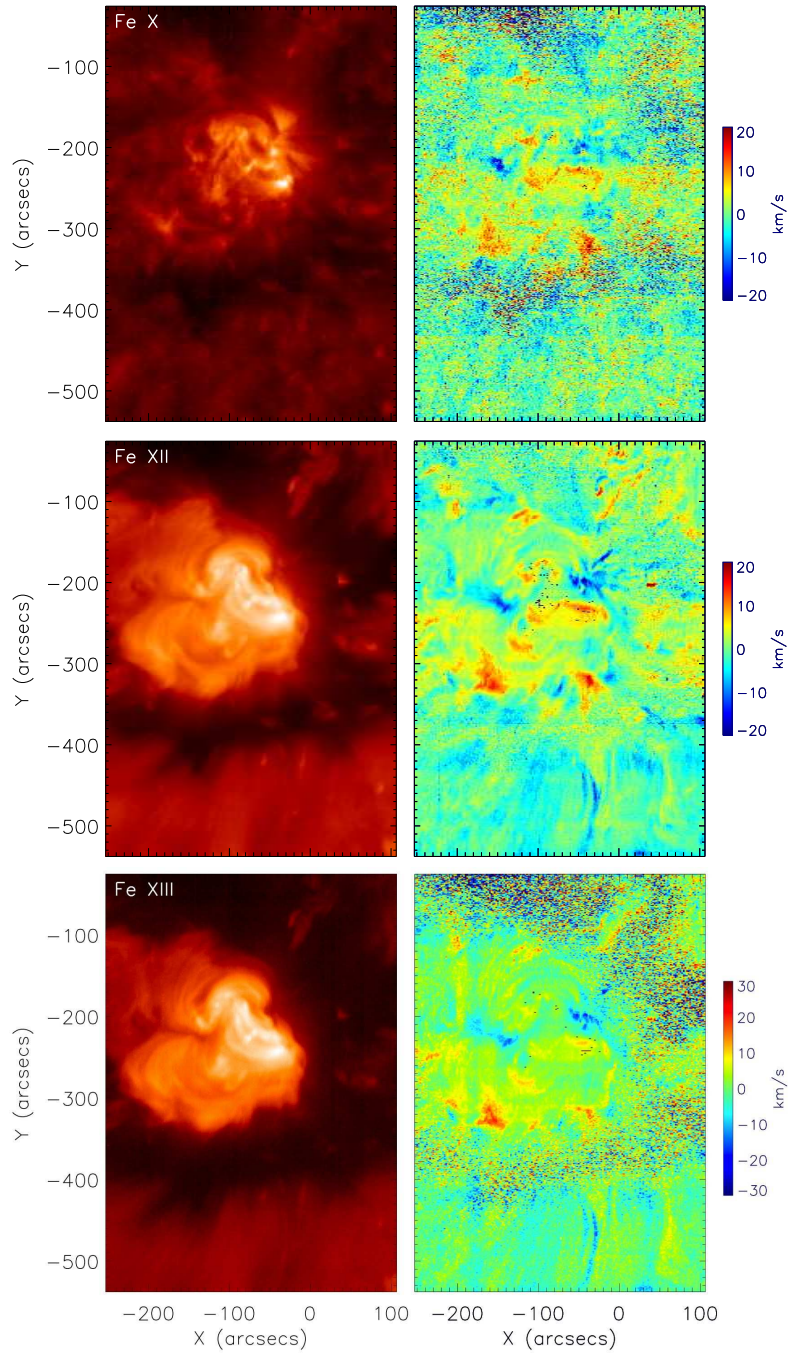
Figure 8. Fe X, Fe XII, and Fe XIII intensity (left) and velocity (right) maps on 17 October 2007 at 02:47 UT. AR outflows are evident at higher coronal formation temperatures beginning with Fe X. The outflow regions spatially expand with increasing temperature.

areas of positive and negative magnetic field concentration. On 18 October at 00:18 UT, the spatial extent of the outflow region on the western side of the AR has expanded well into the surrounding CH as is evident in Figure 9.

Outflow velocities have intensified significantly as the area of the outflow region has increased. Figure 10 contains histograms of velocities in the AR's eastern and western outflow regions for eight EIS rasters. The thick red lines in the top and middle plots represent the average probability distribution function (PDF) of the outflow velocities of the respective regions for the seven rasters in the period 15 to 17 October. The scatter of individual raster's PDFs is relatively small on the eastern side of the AR. On the western side, outflow velocity PDFs are consistent for rasters from 15 to 17 October, however, velocities for 18 October at 00:18 UT have significantly increased across the range of a few to 20 km s^{-1}. The bottom panel in Figure 10 shows the PDF excess of the velocity PDF for 18 October on the western side of the AR over the average velocity PDF of the first seven rasters. The frequency of velocities in the range of 5 to 15 km s^{-1} has more than doubled and the distribution tail has extended to 20 from 13-14 km s^{-1}. This striking intensification in outflow velocities on the 18th was observed in all other hotter coronal lines with sufficient counts.

6. Summary of Observations

The following is a summary of the multiple-instrument observations made of the AR-CH complex from 15 to 18 October:

- A decaying AR embedded in a CH showed a significant magnetic flux decrease of 9.7% per day between 15 to 18 October.
- The coronal loops became increasing sheared and sigmoidal in soft X-rays by 18:00 UT on 17 October.
- EIS velocity maps of the AR-CH complex showed blue-shifted outflows at the periphery of the AR that were persistent during four days of EIS observations.
- Outflow velocities range from a few to 13 km s^{-1} from 15 to 17 October.
- The strongest outflows are spatially coincident with areas of magnetic field concentrations of a single polarity.
- AR outflows are identifiable in hotter coronal lines such as Fe X, Fe XII, and Fe XIII but are much less pronounced or virtually non-existent in cooler lines such as He II, Mg VII and Si VII.
- At 00:18 UT on 18 October, histograms of velocities in outflow regions display a distinct intensification in outflow velocities to 20 km s^{-1} on the western side of the AR where there is a filament lying along the PIL. Similar intensification in outflow velocities occurred in all other unblended coronal lines where sufficient data count rates were available.
- The AR erupted at approximately 07:30 UT on the 18th. Classic on-disk signatures of CMEs are observed in STEREO EUVI, *Hinode* XRT, and TRACE data including, expanding sigmoidal loop structures, dimming regions, and post-eruption loop arcades.
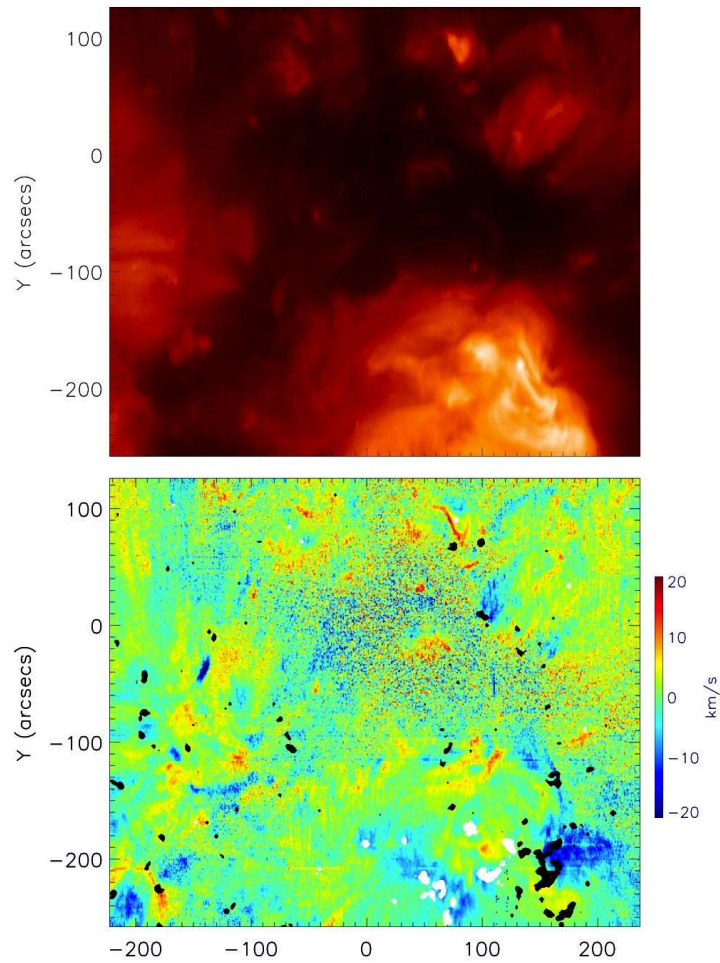- A slow CME was observed in LASCO C2 Coronagraph first seen at 09:06 UT.

Figure 9. EIS Fe XII emission line intensity (top) and velocity (bottom) maps at 00:18 UT on 18 October, approximately six hours before the CME. Velocity map is overlaid with SOHO MDI magnetic field contours of ± 100 G (white/black contours). The outflow regions have expanded on both sides of the AR, especially on the western side where the CME onset takes place. The spatial extension into the nearby CH field on the west occurs as LOS outflow velocities intensify.
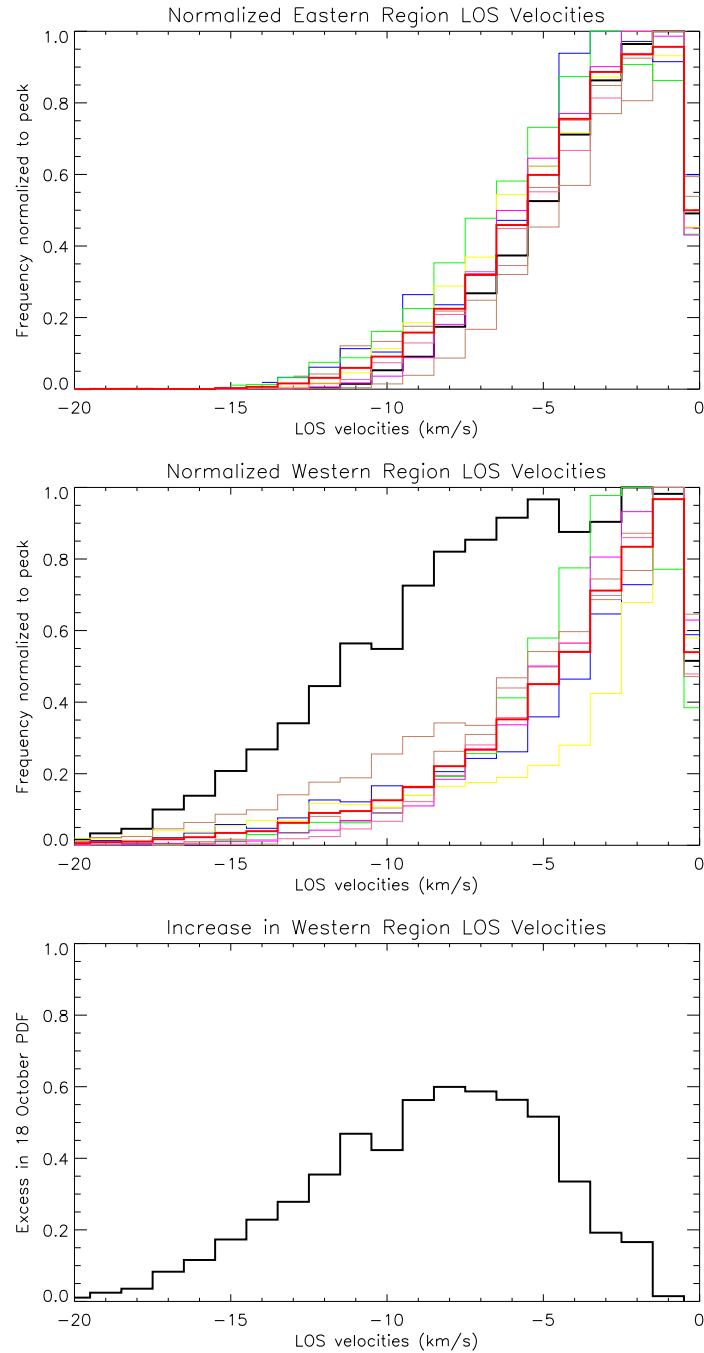
Figure 10. LOS velocity PDFs of eastern (top) and western (middle) outflow regions for each raster, normalized to peak velocities within each velocity bin. Thick black lines are the velocity PDFs from 18 October 2007 00:18 UT, six hours prior to the CME, and thick red lines are the average of the velocity PDFs for all rasters from 15 October 2007 20:39 UT to 17 October 02:47 UT (excludes 18 October 2007 00:18 UT). On the eastern side of the AR, velocity PDFs are approximately similar from 15 October 2007 20:39 UT to 18 October 2007 00:18 UT, however, western region velocity PDF is significantly enhanced at 18 October 00:18 UT compared with velocity PDFs in previous rasters and those on the eastern side. The extent of the enhancement in normalized western region LOS velocities is clearly evident in the bottom panel which shows the excess in the velocity PDF for 18 October 2007 00:18 UT vs the average of the previous velocity PDFs.

7. Simulations

3D MHD simulations replicating the observed AR-CH complex i.e. the magnetic field configuration and field strength were carried out by Murray *et al.* (2010) to investigate the possible origin and driver of AR outflows. The AR inside an equatorial CH provided an opportunity to investigate the possible drivers of outflows with two different magnetic field alignments at the AR-surrounding interfaces, one of which is advantageous for reconnection and the other which is not. On the solar eastern side, the AR's positive polarity is oppositely aligned with the CH's negative field and the magnetic configuration is conducive for reconnection. However, on the western side, the respective polarities are parallel so that fast reconnection is not expected to take place.

Vertical slices through the simulation domain show that on the AR's eastern side, there is a region of high gas pressure and low magnetic pressure, which is characteristic of a current sheet. Reconnection ultimately sets in on this side of the AR, forming closed loops of an anemone structure. No such indications of a current sheet and reconnection are evident on the western side of the AR. A close examination of the forces generated in the CH field reveals the driving mechanism of the outflows in the absence of reconnection. The outflows occur simply as a consequence of the horizontal expansion of the AR which compresses and deforms the nearby CH field as well as compressing the plasma amassed in the CH field. The compressive effects result in enhanced gas pressure gradients against gravitational forces along the 'open' CH field. Only gas pressure gradients can drive the outflows along the CH field because it alone acts in a direction parallel to the magnetic field. Due to the expansion of the AR, the enhanced gas pressure is not fully balanced by the gravitational force, consequently, the plasma in the CH field is accelerated upwards to become outflows.

Confined to the magnetic field lines in the low plasma β environment of the corona, outflowing plasma is accelerated in and along the CH field immediately surrounding the AR. As the AR expands, it pushes the nearby CH field which curves around the AR's loops so that as the outflows rise they follow the curve and expansion of the CH field (Murray *et al.*, 2010). The velocity of the outflowing plasma is dependent upon the relative size of the components of the enhanced gas pressure gradient and gravitational force that are parallel to the CH field. Faster velocities result from larger imbalances in the forces. In summary, larger expansion forces lead to greater compression along the CH field which in turn results in larger gas pressure gradients and faster outflows.

8. Discussion

AR outflows have received much attention since early observations with TRACE (Winebarger, DeLuca, and Golub, 2001). A new view of outflows is being developed through the use of spectroscopic data, in particular with EIS. It was reported by Uchida *et al.* (1992) in the Yohkoh era that ARs can be in a state of continuous expansion. Simulations carried out by Murray *et al.* (2010) show that where surrounding field lines are nearly parallel, continuous, gentle outflows

occur at the periphery of the AR as a result of its expansion. Although the expansion of the AR as a mechanism which accelerates the outflows provides an adequate explanation for the observations, it is unlikely to be working in isolation of reconnection-related mechanisms.

Suggested reconnection mechanisms for outflows include impulsive heating through nano-flare activity at AR loop footpoints (Hara *et al.*, 2008), chromospheric evaporation resulting from continual flux emergence, motion and field line braiding (del Zanna *et al.*, 2006), and expansion of large-scale reconnecting loops (Harra *et al.*, 2008). A unifying concept for the reconnection mechanisms is that of reconnection along quasi-separatrix layers (QSLs) which are preferential locations for current formation and reconnection (Baker *et al.*, 2009a).

Large-scale coronal circulation has also been proposed as an outflow mechanism (Marsch, 2006). In this case outflows are the upward counterpart of a continual mass loss and mass supply to the corona. Propagating density fluctuations along plume structures (Ofman *et al.*, 1997) may also be related to AR outflows as suggested by their spatial coincidence and comparable velocities, although this area needs further study (de Moortel, 2009).

The fact that for four days continuous outflows are observed in EIS rasters on both sides of the AR in our study, irrespective of the relative orientation of the magnetic field lines of the AR and the CH, suggests that mechanisms other than reconnection are also involved in driving outflows. In actuality, AR expansion can lead to the concentration of current sheets by compression and current generation sufficient for reconnection to take place so that it may be possible to simultaneously produce outflows by both driving mechanisms i.e. reconnection and field compression. During the observation period, the principal outflows are located where there are drastic connectivity changes of coronal loops, in the center of the anemone of the AR loops, along the CH-quiet Sun boundary, and between closed loops of the AR and 'open' CH field lines, reinforcing the QSL reconnection-driven outflow scenario (Baker *et al.*, 2009a). However, the extension of the western outflow region well into the 'open' fields of the CH suggests that along the western boundary, compression driven outflows are present. Thus, a combination of driving mechanisms is a plausible explanation for the observed outflows with velocities ranging from a few to 13 km s^{-1} that persisted for four days on both sides of the AR in the CH.

In this AR, the new observation of an intensification of outflow velocities, rather than steady flows, observed on the western side of the AR requires further investigation. What set of circumstances could lead to the enhancement of velocities observed within the AR-CH complex at a particular time and in a specific location? A key result of the 3D MHD simulations provides a viable mechanism for the enhanced velocities observed on 18 October at 00:18 UT on the western side of the AR. In the simulations, greater compressive forces lead to faster outflows. Expansion of a flux rope containing a filament located closer to the western side of the AR is a possible source of additional compressive forces.

A reverse S-shaped pre-eruption filament indicated by yellow arrows in the TRACE 171 Å images in Figure 3 is located above the PIL that lies very close to the western outflow region of the AR (*cf.* Figure 9). At approximately 17:30 UT on 17 October, the eastern portion of the filament begins to erupt and in the

process, the overlying loops disappear in STEREO EUVI 195 Å images by about 18:30 UT. Though STEREO images clearly show that the filament or at least a portion of it begins to erupt, a filament is again visible in TRACE 171 Å data early on the 18th. The reappearance of the filament suggests there was either a failed (confined) or partial eruption. The fact that no CME was apparent in SOHO LASCO C2 observations attributable to the eruption suggests a failed filament eruption may have occurred. The AR-filament complex goes through what appears to be another failed eruption close to the AR's core at 04:30 UT on the 18th when the northeastern portion of the sigmoid expands, before finally erupting at 07:35 UT on the 18th towards the SW, leading to the CME seen in LASCO's C2.

A partial or full CME eruption further changes the coronal field configuration within the AR-CH complex. The reconnection process between the closed AR loops and the 'open' field lines of the CH gradually removes stabilizing field lines from above the highly sheared inversion line, where a filament is present, thus weakening the overlying field, setting the stage for a magnetic breakout and facilitating CME activity. Expansion of the rising filament in the confined eruption on 17 October is likely to force reconnection on the eastern side of the AR between the antiparallel magnetic field of the positive polarity of the AR and the negative polarity of the surrounding CH. The 'open' field of the CH is transported to the western side thus some of the stabilizing overlying field is likely to be removed. The failed eruption at the core of the AR three hours prior to the full-fledged CME will further remove stabilizing field. In fact, both eruptions accelerate what is an ongoing process of the removal of stabilizing overlying field by interchange reconnection (Crooker, Gosling, and Kahler, 2002). This has consequences for the full CME eruption observed hours later (Török and Kliem, 2007).

Examination of time sequences of MDI magnetograms showed that opposite polarity flux converges in the vicinity of the filament hours before the NE expansion and again, early on the 18th, prior to the failed and main eruptions. The flux cancellation indicates the formation of a flux rope including the filament along the main inversion line (van Ballegooijen and Martens, 1989). Location of the flux cancellation on the 18th is spatially coincident with the center of the sigmoid that forms before the CME and which brightens during the CME eruption. Measurements of the flux values from MDI magnetograms show that flux falls by $\approx 10^{21}$ Mx, or 9.7% of total flux per day, throughout the expansion of the AR and series of eruptions, destabilizing tied-down field by flux cancellation and increasing twist in the flux rope since the submerging flux takes away very little helicity while the total flux is decreasing, resulting in the AR becoming increasingly non-potential (van Ballegooijen and Mackay, 2007). Of course flux is cancelled along the entire boundary of the AR's positive field, however, along the main PIL, where the filament is located, flux cancellation involves the strongest magnetic field.

Recent 3D MHD simulations have shown flux cancellation leading to the formation and subsequent eruption of a flux rope in a sheared arcade configuration (Aulanier *et al.* (2010) and references therein). This can occur when flux cancellation is treated as a consequence of photospheric turbulent diffusion such

as in a decaying AR (Amari *et al.*, 2010). In the 3D flux cancellation model of Aulanier *et al.* (2010), photospheric reconnection in a bald-patch separatrix transforms a flux rope lying low in the atmosphere into a slowly rising and stable flux rope. Once a flux rope is formed in the solar atmosphere various models describe how the transition to eruption occurs e.g. torus instability (Aulanier *et al.*, 2010). For a specific case in which the initial state is quite sheared, Amari *et al.* (2010) found that the formation of a twisted flux rope and the subsequent disruption of the configuration can occur when flux has decreased by a relatively small amount over a portion of the AR. Substantial flux cancellation took place in the AR-CH complex leading to the CME.

Observational studies and modelling show that filaments that are about to erupt may exhibit two distinct phases (Moore *et al.* (2001), Moore and Sterling (2006), Schrijver *et al.* (2008) and references therein). The initial phase is characterized by a slow-rise during which both the filament and overlying field expand with velocities from 1 to 15 km s^{-1} (Schrijver *et al.*, 2008). A rapid-acceleration phase follows the slow-rise where velocities increase to a range of 100 up to over 1000 km s^{-1} (Schrijver *et al.*, 2008). Pre-eruption expansion of the flux rope containing the filament located on the western side of the AR could provide the required increase in compressive forces causing intensification of outflows from less than 13 km s^{-1} to 20 km s^{-1} observed in the EIS velocity map at 00:18 UT on the 18th. This suggests that intensification of outflows in parallel with the formation of a sigmoid prior to eruptive activity in the AR-CH complex may be a new class of pre-CME signatures which has implications for space weather predications, if verified in future work. Its precursor status is reinforced by being combined with other well known precursors like sigmoids, persistent cancellation along the PIL, and pre-eruption activity. The MHD model of the AR-CH complex was constructed in an 'open' field environment, but compression induced plasma flows can be created in a closed-loop environment, as was discussed in Murray *et al.* (2010), therefore, intensification of AR outflows may be a generally valid CME precursor. Intensification of outflows resulting from compression should not be limited to ARs. In fact, it may be possible along quiescent filament channels. To be a viable tool for CME forecasts, outflow intensification events have to be recognized within a few hours. The current data acquisition and data reduction methods make this presently impossible. However, slitless spectrographs like the rocket-flown MOSES design (Fox, Kankelborg, and Thomas, 2010), if realized in the future, would make this class of precursor a viable tool for CME forecasting.

9. Conclusion

This work studies the evolution of an AR over four days in which a magnetic flux rope forms and subsequently erupts. Six hours before the eruption, we found a striking increase in outflow velocities in the AR which is surrounded by a CH. The generation of intensified flows is explained by Murray *et al.* (2010) who showed that compression of the nearby CH field by the expanding AR leads to outflows in field rooted in a same-polarity configuration. The AR studied here exhibits a sigmoidal shape indicating that a flux rope is present. The slow-rise and

expansion of this flux rope prior to its eruption would, therefore, logically lead to stronger compression of the surrounding field and intensification of outflows, though it is possible that other, reconnection-related, mechanisms may also play a role. We believe that the intensification of outflows at the edge of this AR is a precursor of its CME. Future work should study the evolution of flows from ARs which contain a sigmoid. Sigmoidal ARs are known to be highly likely to erupt on the time-scales of days following the sigmoid formation. However, the intensification of outflows takes place over only a few hours before the eruption and so may provide a more imminent precursor signature than sigmoids.

References

Amari, T., Aly, J., Mikic, Z., Linker, J.: 2010, Coronal Mass Ejection Initiation: On the Nature of the Flux Cancellation Model. *Astrophys. J. Lett.* **717**, 26 – 30. doi:10.1088/2041-8205/717/1/L26.

Asai, A., Shibata, K., Hara, H., Nitta, N.V.: 2008, Characteristics of Anemone Active Regions Appearing in Coronal Holes Observed with the Yohkoh Soft X-Ray Telescope. *Astrophys. J.* **673**, 1188 – 1193. doi:10.1086/523842.

Asai, A., Shibata, K., Ishii, T.T., Oka, M., Kataoka, R., Fujiki, K., Gopalswamy, N.: 2009, Evolution of the anemone AR NOAA 10798 and the related geo-effective flares and CMEs. *J. Geophys. Res.* **114**, A00A21. doi:10.1029/2008JA013291.

Aulanier, G., Démoulin, P., Grappin, R.: 2005, Equilibrium and observational properties of line-tied twisted flux tubes. *Astron. Astrophys.* **430**, 1067 – 1087. doi:10.1051/0004-6361:20041519.

Aulanier, G., Török, T., Démoulin, P., DeLuca, E.E.: 2010, Formation of Torus-Unstable Flux Ropes and Electric Currents in Erupting Sigmoids. *Astrophys. J.* **708**, 314 – 333. doi:10.1088/0004-637X/708/1/314.

Baker, D., van Driel-Gesztelyi, L., Mandrini, C.H., Démoulin, P., Murray, M.J.: 2009a, Magnetic Reconnection along Quasi-separatrix Layers as a Driver of Ubiquitous Active Region Outflows. *Astrophys. J.* **705**, 926 – 935. doi:10.1088/0004-637X/705/1/926.

Baker, D., Rouillard, A.P., van Driel-Gesztelyi, L., Démoulin, P., Harra, L.K., Lavraud, B., Davies, J.A., Opitz, A., Luhmann, J.G., Sauvaud, J.-A., Galvin, A.B.: 2009b, Signatures of interchange reconnection: STEREO, ACE and Hinode observations combined. *Ann. Geophysicae* **27**, 3883 – 3897. doi:10.5194/angeo-27-3883-2009.

Brooks, D.H., Warren, H.P.: 2011, Establishing a Connection Between Active Region Outflows and the Solar Wind: Abundance Measurements with EIS/Hinode. *Astrophys. J. Lett.* **727**, L13+. doi:10.1088/2041-8205/727/1/L13.

Brueckner, G.E., Howard, R.A., Koomen, M.J., Korendyke, C.M., Michels, D.J., Moses, J.D., Socker, D.G., Dere, K.P., Lamy, P.L., Llebaria, A., Bout, M.V., Schwenn, R., Simnett, G.M., Bedford, D.K., Eyles, C.J.: 1995, The Large Angle Spectroscopic Coronagraph (LASCO). *Solar Phys.* **162**, 357 – 402. doi:10.1007/BF00733434.

Bryans, P., Young, P.R., Doschek, G.A.: 2010, Multiple Component Outflows in an Active Region Observed with the EUV Imaging Spectrometer on Hinode. *Astrophys. J.* **715**, 1012 – 1020. doi:10.1088/0004-637X/715/2/1012.

Canfield, R.C., Hudson, H.S., McKenzie, D.E.: 1999, Sigmoidal morphology and eruptive solar activity. *Geophys. Res. Lett.* **26**, 627 – 630. doi:10.1029/1999GL900105.

Chen, P.F., Innes, D.E., Solanki, S.K.: 2008, SOHO/SUMER observations of prominence oscillation before eruption. *Astron. Astrophys.* **484**, 487 – 493. doi:10.1051/0004-6361:200809544.

Chifor, C., Mason, H.E., Tripathi, D., Isobe, H., Asai, A.: 2006, The early phases of a solar prominence eruption and associated flare: a multi-wavelength analysis. *Astron. Astrophys.* **458**, 965 – 973. doi:10.1051/0004-6361:20065687.

Chifor, C., Tripathi, D., Mason, H.E., Dennis, B.R.: 2007, X-ray precursors to flares and filament eruptions. *Astron. Astrophys.* **472**, 967 – 979. doi:10.1051/0004-6361:20077771.

Crooker, N.U., Gosling, J.T., Kahler, S.W.: 2002, Reducing heliospheric magnetic flux from coronal mass ejections without disconnection. *J. Geophys. Res.* **107 (A2) SSH 3-1**.

Culhane, J.L., Harra, L.K., James, A.M., Al-Janabi, K., Bradley, L.J., Chaudry, R.A., Rees, K., Tandy, J.A., Thomas, P., Whillock, M.C.R., Winter, B., Doschek, G.A., Korendyke, C.M., Brown, C.M., Myers, S., Mariska, J., Seely, J., Lang, J., Kent, B.J., Shaughnessy, B.M., Young, P.R., Simnett, G.M., Castelli, C.M., Mahmoud, S., Mapson-Menard, H., Probyn, B.J., Thomas, R.J., Davila, J., Dere, K., Windt, D., Shea, J., Hagood, R., Moye, R., Hara, H., Watanabe, T., Matsuzaki, K., Kosugi, T., Hansteen, V., Wikstol, Ø.: 2007, The EUV Imaging Spectrometer for Hinode. *Solar Phys.* **243**, 19 – 61. doi:10.1007/s01007-007-0293-1.

de Moortel, I.: 2009, Longitudinal Waves in Coronal Loops. *Space Sci. Rev.* **149**, 65 – 81. doi:10.1007/s11214-009-9526-5.

Del Zanna, G.: 2008, Flows in active region loops observed by Hinode EIS. *Astron. Astrophys.* **481**, 49 – 52. doi:10.1051/0004-6361:20079087.

del Zanna, G., Schmieder, B., Mason, H., Berlicki, A., Bradshaw, S.: 2006, The Gradual Phase of the X17 Flare on October 28, 2003. *Solar Phys.* **239**, 173 – 191. doi:10.1007/s11207-006-0184-4.

Dere, K.P., Brueckner, G.E., Howard, R.A., Koomen, M.J., Korendyke, C.M., Kreplin, R.W., Michels, D.J., Moses, J.D., Moulton, N.E., Socker, D.G., St. Cyr, O.C., Delaboudinière, J.P., Artzner, G.E., Brunaud, J., Gabriel, A.H., Hochedez, J.F., Millier, F., Song, X.Y., Chauvineau, J.P., Marioge, J.P., Defise, J.M., Jamar, C., Rochus, P., Catura, R.C., Lemen, J.R., Gurman, J.B., Neupert, W., Clette, F., Cugnon, P., van Dessel, E.L., Lamy, P.L., Llebaria, A., Schwenn, R., Simnett, G.M.: 1997, EIT and LASCO Observations of the Initiation of a Coronal Mass Ejection. *Solar Phys.* **175**, 601 – 612. doi:10.1023/A:1004907307376.

Doschek, G.A., Warren, H.P., Mariska, J.T., Muglach, K., Culhane, J.L., Hara, H., Watanabe, T.: 2008, Flows and Nonthermal Velocities in Solar Active Regions Observed with the EUV Imaging Spectrometer on Hinode: A Tracer of Active Region Sources of Heliospheric Magnetic Fields? *Astrophys. J.* **686**, 1362 – 1371. doi:10.1086/591724.

Feynman, J., Martin, S.F.: 1995, The initiation of coronal mass ejections by newly emerging magnetic flux. *J. Geophys. Res.* **100**, 3355 – 3367. doi:10.1029/94JA02591.

Foullon, C., Verwichte, E., Nakariakov, V.M.: 2009, Ultra-long-period Oscillations in EUV Filaments Near to Eruption: Two-wavelength Correlation and Seismology. *Astrophys. J.* **700**, 1658 – 1665. doi:10.1088/0004-637X/700/2/1658.

Fox, J.L., Kankelborg, C.C., Thomas, R.J.: 2010, A Transition Region Explosive Event Observed in He II with the MOSES Sounding Rocket. *Astrophys. J.* **719**, 1132 – 1143. doi:10.1088/0004-637X/719/2/1132.

Gary, G.A., Moore, R.L.: 2004, Eruption of a Multiple-Turn Helical Magnetic Flux Tube in a Large Flare: Evidence for External and Internal Reconnection That Fits the Breakout Model of Solar Magnetic Eruptions. *Astrophys. J.* **611**, 545 – 556. doi:10.1086/422132.

Glover, A., Ranns, N.D.R., Harra, L.K., Culhane, J.L.: 2000, The Onset and Association of CMEs with Sigmoidal Active Regions. *Geophys. Res. Lett.* **27**, 2161 – 2164. doi:10.1029/2000GL000018.

Golub, L., Deluca, E., Austin, G., Bookbinder, J., Caldwell, D., Cheimets, P., Cirtain, J., Cosmo, M., Reid, P., Sette, A., Weber, M., Sakao, T., Kano, R., Shibasaki, K., Hara, H., Tsuneta, S., Kumagai, K., Tamura, T., Shimojo, M., McCracken, J., Carpenter, J., Haight, H., Siler, R., Wright, E., Tucker, J., Rutledge, H., Barbera, M., Peres, G., Varisco,

S.: 2007, The X-Ray Telescope (XRT) for the Hinode Mission. *Solar Phys.* **243**, 63–86. doi:10.1007/s11207-007-0182-1.

Gopalswamy, N., Mikić, Z., Maia, D., Alexander, D., Cremades, H., Kaufmann, P., Tripathi, D., Wang, Y.: 2006, The Pre-CME Sun. *Space Sci. Rev.* **123**, 303–339. doi:10.1007/s11214-006-9020-2.

Green, L.M., Kliem, B.: 2009, Flux Rope Formation Preceding Coronal Mass Ejection Onset. *Astrophys. J. Lett.* **700**, 83–87. doi:10.1088/0004-637X/700/2/L83.

Green, L.M., Démoulin, P., Mandrini, C.H., Van Driel-Gesztelyi, L.: 2003, How are Emerging Flux, Flares and CMEs Related to Magnetic Polarity Imbalance in MDI Data? *Solar Phys.* **215**, 307–325.

Green, L.M., Kliem, B., Török, T., van Driel-Gesztelyi, L., Attrill, G.D.R.: 2007, Transient Coronal Sigmoids and Rotating Erupting Flux Ropes. *Solar Phys.* **246**, 365–391. doi:10.1007/s11207-007-9061-z.

Handy, B.N., Acton, L.W., Kankelborg, C.C., Wolfson, C.J., Akin, D.J., Bruner, M.E., Caravalho, R., Catura, R.C., Chevalier, R., Duncan, D.W., Edwards, C.G., Feinstein, C.N., Freeland, S.L., Friedlaender, F.M., Hoffmann, C.H., Hurlburt, N.E., Jurcevich, B.K., Katz, N.L., Kelly, G.A., Lemen, J.R., Levay, M., Lindgren, R.W., Mathur, D.P., Meyer, S.B., Morrison, S.J., Morrison, M.D., Nightingale, R.W., Pope, T.P., Rehse, R.A., Schrijver, C.J., Shine, R.A., Shing, L., Strong, K.T., Tarbell, T.D., Title, A.M., Torgerson, D.D., Golub, L., Bookbinder, J.A., Caldwell, D., Cheimets, P.N., Davis, W.N., Deluca, E.E., McMullen, R.A., Warren, H.P., Amato, D., Fisher, R., Maldonado, H., Parkinson, C.: 1999, The transition region and coronal explorer. *Solar Phys.* **187**, 229–260. doi:10.1023/A:1005166902804.

Hara, H., Watanabe, T., Harra, L.K., Culhane, J.L., Young, P.R., Mariska, J.T., Doschek, G.A.: 2008, Coronal Plasma Motions near Footpoints of Active Region Loops Revealed from Spectroscopic Observations with Hinode EIS. *Astrophys. J. Lett.* **678**, 67–71. doi:10.1086/588252.

Harra, L.K., Démoulin, P., Mandrini, C.H., Matthews, S.A., van Driel-Gesztelyi, L., Culhane, J.L., Fletcher, L.: 2005, Flows in the solar atmosphere due to the eruptions on the 15th July, 2002. *Astron. Astrophys.* **438**, 1099–1106. doi:10.1051/0004-6361:20052965.

Harra, L.K., Sakao, T., Mandrini, C.H., Hara, H., Imada, S., Young, P.R., van Driel-Gesztelyi, L., Baker, D.: 2008, Outflows at the Edges of Active Regions: Contribution to Solar Wind Formation? *Astrophys. J. Lett.* **676**, 147–150. doi:10.1086/587485.

Harrison, R.A.: 1986, Solar coronal mass ejections and flares. *Astron. Astrophys.* **162**, 283–291.

Harrison, R.A., Waggett, P.W., Bentley, R.D., Phillips, K.J.H., Bruner, M., Dryer, M., Simnett, G.M.: 1985, The X-ray signature of solar coronal mass. *Solar Phys.* **97**, 387–400. doi:10.1007/BF00165998.

Hudson, H.S., Lemen, J.R., St. Cyr, O.C., Sterling, A.C., Webb, D.F.: 1998, X-ray coronal changes during halo CMEs. *Geophys. Res. Lett.* **25**, 2481–2484. doi:10.1029/98GL01303.

Jackson, B.V., Sheridan, K.V., Dulk, G.A., McLean, D.J.: 1978, A possible association of solar type III bursts and white light transients. *Proc. Astron. Soc. Aust.* **3**, 241–242.

Leamon, R.J., Canfield, R.C., Pevtsov, A.A.: 2002, Properties of magnetic clouds and geomagnetic storms associated with eruption of coronal sigmoids. *J. Geophys. Res.* **107 (A9) SSH 1-1**.

Marsch, E.: 2006, Solar wind responses to the solar activity cycle. *Adv. Space Res.* **38**, 921–930. doi:10.1016/j.asr.2005.07.029.

Moore, R.L., Sterling, A.C.: 2006, Initiation of Coronal Mass Ejections. In: N.. Gopalswamy, R. Mewaldt, & J. Torsti (ed.) *Solar Eruptions and Energetic Particles*, *AGU Geophysical Monograph* **165**, 43.

Moore, R.L., Sterling, A.C., Hudson, H.S., Lemen, J.R.: 2001, Onset of the Magnetic Explosion in Solar Flares and Coronal Mass Ejections. *Astrophys. J.* **552**, 833–848. doi:10.1086/320559.

Murray, M.J., Baker, D., van Driel-Gesztelyi, L., Sun, J.: 2010, Outflows at the Edges of an Active Region in a Coronal Hole: A Signature of Active Region Expansion? *Solar Phys.* **261**, 253–269. doi:10.1007/s11207-009-9484-9.

Ofman, L., Romoli, M., Poletto, G., Noci, G., Kohl, J.L.: 1997, Ultraviolet Coronagraph Spectrometer Observations of Density Fluctuations in the Solar Wind. *Astrophys. J. Lett.* **491**, 111–114. doi:10.1086/311067.

Peter, H.: 2010, Asymmetries of solar coronal extreme ultraviolet emission lines. *ArXiv e-prints*.

Pevtsov, A.A., Canfield, R.C., McClymont, A.N.: 1997, On the Subphotospheric Origin of Coronal Electric Currents. *Astrophys. J.* **481**, 973 – 977. doi:10.1086/304065.

Pick, M., Forbes, T.G., Mann, G., Cane, H.V., Chen, J., Ciaravella, A., Cremades, H., Howard, R.A., Hudson, H.S., Klassen, A., Klein, K.L., Lee, M.A., Linker, J.A., Maia, D., Mikic, Z., Raymond, J.C., Reiner, M.J., Simnett, G.M., Srivastava, N., Tripathi, D., Vainio, R., Vourlidas, A., Zhang, J., Zurbuchen, T.H., Sheeley, N.R., Marqué, C.: 2006, Multi-Wavelength Observations of CMEs and Associated Phenomena. Report of Working Group F. *Space Sci. Rev.* **123**, 341 – 382. doi:10.1007/s11214-006-9021-1.

Ramsey, H.E., Smith, S.F.: 1966, Flare-initiated filamei it oscillations. *Astron. J.* **71**, 197 – 199. doi:10.1086/109903.

Rust, D.M., Kumar, A.: 1996, Evidence for Helically Kinked Magnetic Flux Ropes in Solar Eruptions. *Astrophys. J. Lett.* **464**, 199 – 202. doi:10.1086/310118.

Sakao, T., Kano, R., Narukage, N., Kotoku, J., Bando, T., DeLuca, E.E., Lundquist, L.L., Tsuneta, S., Harra, L.K., Katsukawa, Y., Kubo, M., Hara, H., Matsuzaki, K., Shimojo, M., Bookbinder, J.A., Golub, L., Korreck, K.E., Su, Y., Shibasaki, K., Shimizu, T., Nakatani, I.: 2007, Continuous Plasma Outflows from the Edge of a Solar Active Region as a Possible Source of Solar Wind. *Science* **318**, 1585 – 1588. doi:10.1126/science.1147292.

Scherrer, P.H., Bogart, R.S., Bush, R.I., Hoeksema, J.T., Kosovichev, A.G., Schou, J., Rosenberg, W., Springer, L., Tarbell, T.D., Title, A., Wolfson, C.J., Zayer, I., MDI Engineering Team: 1995, The Solar Oscillations Investigation - Michelson Doppler Imager. *Solar Phys.* **162**, 129 – 188. doi:10.1007/BF00733429.

Schrijver, C.J., Elmore, C., Kliem, B., Török, T., Title, A.M.: 2008, Observations and Modeling of the Early Acceleration Phase of Erupting Filaments Involved in Coronal Mass Ejections. *Astrophys. J.* **674**, 586 – 595. doi:10.1086/524294.

Shibata, K., Nitta, N., Strong, K.T., Matsumoto, R., Yokoyama, T., Hirayama, T., Hudson, H., Ogawara, Y.: 1994, A gigantic coronal jet ejected from a compact active region in a coronal hole. *Astrophys. J. Lett.* **431**, 51 – 53. doi:10.1086/187470.

Sterling, A.C., Hudson, H.S.: 1997, YOHKOH SXT Observations of X-Ray "Dimming" Associated with a Halo Coronal Mass Ejection. *Astrophys. J. Lett.* **491**, 55 – 58. doi:10.1086/311043.

Sterling, A.C., Moore, R.L.: 2005, Slow-Rise and Fast-Rise Phases of an Erupting Solar Filament, and Flare Emission Onset. *Astrophys. J.* **630**, 1148 – 1159. doi:10.1086/432044.

Titov, V.S., Démoulin, P.: 1999, Basic topology of twisted magnetic configurations in solar flares. *Astron. Astrophys.* **351**, 707 – 720.

Török, T., Kliem, B.: 2007, Numerical simulations of fast and slow coronal mass ejections. *Astron. Nachr.* **328**, 743 – 746. doi:10.1002/asna.200710795.

Uchida, Y., McAllister, A., Strong, K.T., Ogawara, Y., Shimizu, T., Matsumoto, R., Hudson, H.S.: 1992, Continual expansion of the active-region corona observed by the YOHKOH Soft X-ray Telescope. *Publ. Astron. Soc. Japan* **44**, 155 – 160.

van Ballegooijen, A.A., Mackay, D.H.: 2007, Model for the Coupled Evolution of Subsurface and Coronal Magnetic Fields in Solar Active Regions. *Astrophys. J.* **659**, 1713 – 1725. doi:10.1086/512849.

van Ballegooijen, A.A., Martens, P.C.H.: 1989, Formation and eruption of solar prominences. *Astrophys. J.* **343**, 971 – 984. doi:10.1086/167766.

Vršnak, B.: 1993, Classification of Prominence Oscillations. *Hvar Obs. Bull.* **17**, 23 – .

Williams, D.R., Török, T., Démoulin, P., van Driel-Gesztelyi, L., Kliem, B.: 2005, Eruption of a Kink-unstable Filament in NOAA Active Region 10696. *Astrophys. J. Lett.* **628**, 163 – 166. doi:10.1086/432910.

Winebarger, A.R., DeLuca, E.E., Golub, L.: 2001, Apparent Flows above an Active Region Observed with the Transition Region and Coronal Explorer. *Astrophys. J. Lett.* **553**, 81 – 84. doi:10.1086/320496.

Wuelser, J.-P., Lemen, J.R., Tarbell, T.D., Wolfson, C.J., Cannon, J.C., Carpenter, B.A., Duncan, D.W., Gradwohl, G.S., Meyer, S.B., Moore, A.S., Navarro, R.L., Pearson, J.D., Rossi, G.R., Springer, L.A., Howard, R.A., Moses, J.D., Newmark, J.S., Delaboudiniere, J.-P., Artzner, G.E., Auchere, F., Bougnet, M., Bouyries, P., Bridou, F., Clotaire, J.-Y., Colas, G., Delmotte, F., Jerome, A., Lamare, M., Mercier, R., Mullot, M., Ravet, M.-F., Song, X., Bothmer, V., Deutsch, W.: 2004, EUVI: the STEREO-SECCHI extreme ultraviolet imager. In: S. Fineschi & M. A. Gummin (ed.) *Society of Photo-Optical Instrumentation Engineers (SPIE) Conference Series*, *Society of Photo-Optical Instrumentation Engineers (SPIE) Conference Series* **5171**, 111 – 122. doi:10.1117/12.506877.

Young, P.R., Del Zanna, G., Mason, H.E., Dere, K.P., Li, E., Lini, M., Doschek, G.A., Brown, C.M., Culhane, L., Harra, L.K., Watanabe, T., Hara, H.: 2007, EUV Emission Lines and Diagnostics Observed with Hinode/EIS. *Publ. Astron. Soc. Japan* **59**, 857 – 864.
Young, P.R., Watanabe, T., Hara, H., Mariska, J.T.: 2009, High-precision density measurements in the solar corona. I. Analysis methods and results for Fe XII and Fe XIII. *Astron. Astrophys.* **495**, 587 – 606. doi:10.1051/0004-6361:200810143.